GPCR and G protein mobility in D. discoideum : a single molecule study

Hemert, F. van

Chapter 3

Leading edge specific attenuation of cortex / membrane interactions leads to polarized GPCR mobility

Single Molecule Microscopy (SMM) was used to investigate the diffusion of the G Protein Coupled Receptor cAR1 which is responsible for gradient sensing in *Dictyostelium discoideum*. We show that the mobility of cAR1 is globally increased ∼twofold during chemotaxis with respect to naïve (not exposed to cAMP) cells, higher at the leading than at the trailing edge and that this effect requires an intact G protein. Upon disruption of the F-actin cytoskeleton network by latrunculin A (lat A) the mobility of cAR1 also increases twofold indicating either a direct or an indirect interaction with actin filaments and implicating them as a likely regulator of cAR1 mobility. Surprisingly, in lat A treated cells in a cAMP gradient the overall mobility is even higher than in naïve lat A treated cells and cAR1 mobility is still increased at the anterior with respect to the posterior. We propose that F-actin restricts diffusion of cAR1 and that G protein dependent attenuation of F-actin or its interaction with the membrane leads to the polarized cAR1 mobility but clearly other factors involved in gradient sensing are also playing a part.

3.1 Introduction

Tight regulation of the cytoskeleton is vital to a multitude of cellular functions. Proteins that fulfill this task are important in cytokinesis, maintaining cell shape, stabilization of cell-cell and cell-substrate interactions, and regulation of cell motility. The cytoskeleton interactions however do not go one way, signaling molecules, even lipids, can be spatially confined by filamentous actin (F-actin) [94]. Such interactions presumably serve as a feedback between F-actin and its activating molecules and play an important role during directed as well as random cell movement of multiple cell types [80, 42].

In *Dictyostelium discoideum* more than 50% of the obstruction experienced by cytosolic signaling molecules is caused by F-actin [76]. Regarding cell polarization, the relevance of the mobility of signaling molecules on their function was predicted by a diffusion-translocation model [75] and recently confirmed by us in an initial study of receptor mobility [17]. The model concludes that "the capacity of a second messenger to establish and maintain localized signals, is mainly determined by its dispersion range". It is clear that the dispersion range is a function of the messenger's "off-rate" and its diffusion constant. Moreover in the cell membrane in which diffusion is restricted to two dimensions the rate of a reaction involving multiple molecular species is proportional to their concentration and speed [4]. In short, the mobility of signaling components in a polarized system, and any polarity regarding the latter, determines how well such a system can maintain and amplify that polarity. The only way to circumvent signal delocalization of highly mobile signaling molecules while preserving a high reaction rate is compartmentalization. The F-actin cytoskeleton has been suggested numerous times before as candidate to provide for micro-compartments [57, 94, 2].

The social single cell eukaryote *D. discoideum* is a widely used model organism for studying directed cell movement and cytoskeleton dynamics. *D. discoideum* is easily accessible to microscopy, easy to culture, its genome is completely sequenced, and the biochemical networks leading to chemotactic behavior have been extensively characterized. In addition, reliable methods have been developed to observe individual, fluorescence-tagged molecules during chemotaxis [90, 17].

In order to detect a gradient, *D. discoideum* relies on a G protein coupled receptor system making it an interesting model from a physiological perspective as well. The binding of cyclic adenosine mono-phosphate (cAMP) to the *D. discoideum* cAMP receptor 1 (cAR1) promotes the exchange of guanine di-phosphate (GDP) for guanine tri-phosphate (GTP) in the Gα2 subunit of the Gα2$\beta\gamma$ heterotrimer. In the dogmatic view the trimer subsequently dissociates into a Gα2 and a G$\beta\gamma$ subunit. Recently, it has been shown that both G protein subunits continuously cycle between the membrane and the cytosol. Upon stimulation of cAR1, the Gα2 subunit decouples from G$\beta\gamma$ [44, 22] and increases its affinity for the membrane and potentially cAR1 [22]. The G$\beta\gamma$ subunit immobilizes in an F-actin dependent manner (chapter 2) and decouples from cAR1 presumably entering the cytosol [22]. In a cAMP gradient, G protein activation is proportional to the activation of cAR1 [44, 100] along the cell membrane. In addition, G$\beta\gamma$ immobilizes specifically at the leading edge in an F-actin dependent manner (chapter 2). It is known that both G protein subunits have specific downstream targets of which the most important ones for chemotaxis are probably Ras guanine exchange factors (RasGEFs). RasGEFs activate small G proteins of the Ras subfamily in a specific manner. For chemotaxis and cAMP relay, RasC and RasG are the most important proteins of the Ras subfamily [5]. Activation of Ras proteins is the earliest polarized response downstream of G proteins [103] and leads to the polarized activation of PI3K [40, 30], PLA2 [11], TorC2 and subsequently 2 PKB homologues (PKBA and PKBR1) [48]. How exactly the coordinated action of these pathways leads to the spatial regulation of the cytoskeleton that finally results in cell motility still has to be revealed.

In this paper we investigate the role of the F-actin cytoskeleton on the mobility of cAR1. We show that the mobility of cAR1 is decreased in the presence of F-actin. When *D. discoideum* cells chemotax, cAR1 mobility increases globally and likewise in a polarized leading edge *vs* trailing edge manner.

The result of finding a higher receptor mobility at the leading edge, where the abundance of F-actin was shown to be increased, lead us to propose to differentiate between two F-actin types. F-actin that lines the membrane making up the membrane cortex or membrane cytoskeleton, and the F-actin that generates force required for leading edge propulsion. The first type inhibits cAR1 diffusivity. Cortex - membrane

interactions are less tight at the leading edge of chemotaxing *D. discoideum* [64], probably to facilitate the formation of blebs which result in faster cellular movement [101, 58]. The fact that lat A treated cells can still modulate cAR1 mobility in a cAMP gradient suggests that other factors involved in gradient sensing also influence the dynamics of membrane localized signaling molecules.

3.2 Materials and methods

3.2.1 Cell culture and transformation

The axenically growing *D. discoideum* strain Ax2 will be referred to as wildtype (wt). All cells were cultured at 22°C. Wt, $g\alpha 2^-$ (myc2, [13]) and $g\beta^-$ (LW5, [60]) cells were transformed using electroporation with a cAR1-eYFP containing plasmid. We used G418 (Geneticin, Invitrogen) to select for successfully transformed cells, Cells were grown as a monolayer on plastic dishes in axenic culture medium, HL5-C (Formedium), containing 10 µg/ml penicillin/streptomycin (1:1) (Invitrogen) suitably supplemented with 10-20 µg/ml G418.

3.2.2 Preparation of cells for measurements

A confluent 10 cm petridish was incubated overnight in loflo medium (Formedium) to reduce cellular autofluorescence. In the morning, cells were washed once by collecting all cells in 5 ml development buffer (DB, [24]) and spinning down for 4 min at 400$\times$ g RCF. Cells were then resuspended in 5 ml DB and shaken gently at $\sim$100 rpm After 1 hr the cells were pulsed with 150 nM cAMP per pulse every 6 min using a timer and a peristaltic pump for 4 hr. Subsequently the cells were washed again with fresh DB as before and left to shake for 40 min After settling for 20 min on a chambered coverglass (labtek), measurements commenced. All measurements took place in DB at room temperature for a maximum of 2 hr (15-60 sec/cell). The term "naïve" is used for cells that have undergone this treatment but were not further subjected to cAMP (not by global stimulation and not by the application of a cAMP gradient) or lat A.

3.2.3 Global cAMP stimulation assay

The developmental buffer, covering naïve cells in the chambered cover-glasses was supplemented with cAMP to a final concentration of 100 nM or 10 µM. Experiments were performed within either 6 or 20 min after addition of cAMP.

3.2.4 Applied gradient assay

After settling on the coverglass, a micropipette (Eppendorf femtotip) attached to an Eppendorf Femtojet was suspended just above the glass coverslide on which the cells reside. The internal pressure of the Femtojet was set to 40 KPa. This created a stable cAMP gradient of about 10% over the cell body at a mid-concentration of 60 nM as verified experimentally and by simulation. Wt cells polarized within a minute and moved accurately towards the needle. Measurements at the anterior and posterior of polarized cells were taken at a distance of $\sim$70 µm from the pipette tip. The region of interest was set up such that we measured approximately 20% of the cell length at the anterior and posterior (fig.3.1A).

3.2.5 Latrunculin A treatment

The DB in which the cells have settled on the coverglass was supplemented to a final concentration of 0.5 µM lat A. After 10 min of incubation measurements were performed for a maximum of 10 min.

3.2.6 Single-molecule microscopy

The experimental setup for single-molecule imaging has been described in detail previously [81]. The samples were mounted onto an inverted microscope (Axiovert100, Zeiss) equipped with a 100$\times$ objective (NA=1.4, Zeiss) and a sensitive CCD camera. The region-of-interest was set to 50 $\times$ 50 pixels. The apparent pixel size was 220 nm. Measurements were performed by illumination of the samples for 5 ms at 514 nm (Argon-ion laser, Spectra Physics) at an intensity of 2 kW/cm^2. The cells were photobleached for a period of 2-5 sec and sequences of 500 images with a timelag of 50 ms were taken. Use of an appropriate filter combination (Chroma) permitted

the detection of the fluorescence signals on a liquid nitrogen-cooled CCD-camera (Princeton Instruments). The setup allowed us to image individual fluorophores at a signal-to-background-noise ratio of ∼30 leading to a positional accuracy of σ_0 = 40 nm (fig.3.1B).

3.2.7 Analysis of single molecule data

The positions of individual molecules were determined within each image stack by fitting the intensity profiles to a 2D Gaussian using Matlab (Mathworks Inc). The center-of-mass of the Gaussian fit corresponds within ∼40 nm to the position of the molecule. Typically image stacks on 50-200 cells were taken that lead to 2-6 · 10^4 individual molecule positions in each of the experiments shown. The position data were subsequently used to perform particle image correlation spectroscopy (PICS, [83]). PICS calculates the cross-correlation between individual molecule positions at two different points in time (fig.3.1C) from which the cumulative density function ($cdf(r^2, t_{lag})$) of squared displacements was constructed for each timelag (t_{lag}) between 50 and 400 ms (fig.3.1D). At least 2 · 10^4 individual molecules were used to construct the cdfs. The cdfs are subsequently fitted to a two fraction diffusion model:

$$cdf(r^2, t_{lag}) = 1 - \left(\alpha \cdot \exp\left(-\frac{r^2}{MSD_1}\right) + (1-\alpha)\exp\left(-\frac{r^2}{MSD_2}\right)\right) \quad (3.1)$$

The fast fraction size, α, was globally fitted for all timelags in a given data set. This yielded 2 mean squared displacements (MSD_1, MSD_2) per timelag and one fast fraction size for each data set (fig.3.1D). Subsequently the MSDs were plotted versus t_{lag} resulting in a representation of the diffusion behavior. To determine the diffusion constant we fitted each of the MSDs *vs* time datasets to a free diffusion model:

$$MSD = 4Dt_{lag} \quad (3.2)$$

This final analysis yielded two diffusion constants (D_1, D_2) and two offsets (s_0) (fig.3.1E). In the case that two dataset were compared (for example anterior *vs* posterior), MSD_1 and MSD_2 were kept equal per timelag for the two datasets, the fast fraction size (α) was kept constant per dataset but varied between the two data sets

resulting in 2 diffusion constants and two fraction sizes per fit. In this analysis, the fast fraction size α was the only parameter signifying the difference between the two experimental conditions.

The offset s_0 is a representation of the accuracy by which the position of the molecules, σ was determined in each dimension. The positional accuracy leads to the offset in equation 3.2 of $s_0 = 4\sigma^2$ in two dimensions. Given that σ scales with the signal-to-noise ratio ($\sigma = \frac{\frac{\lambda}{2}}{\sqrt{SNR}}$, λ = wavelength of detected light) and since every observation of an individual molecule is achieved at different signal-to-noise ratios, a distribution in σ must be taken into account. For the data presented here $\sigma = 40 \pm 20$ nm. As outlined in the Appendix this distribution in positional accuracies renders the simple expression in the squared displacement analysis of equation 3.1 inaccurate. This becomes important in the case that MSD_1 and MSD_2 are close to σ^2, as presented here. Subsequently the data treatment leads to two different offset values $s_{0,1}$ and $s_{0,2}$ for the fast and slow fraction, respectively. It should be noted that independent of this inaccuracy, the diffusion constants as determined from the slopes of the MSD with timelag were unchanged.

3.2.8 Error estimation

To determine the correct error in the diffusion constants and the fraction size distributions we used bootstrapping. Each dataset was build up from all the observed molecules found in 40-200 individual cells. From the total dataset 30 random subsets were chosen. These resampled sub-sets were subsequently analyzed as describe before, yielding 60 different diffusion constants (2 for each dataset) and 30 fast fraction sizes. The standard deviation of these distributions was taken as an accurate representation of the biological variance among cells and as error estimates for the data obtained on the full data set.

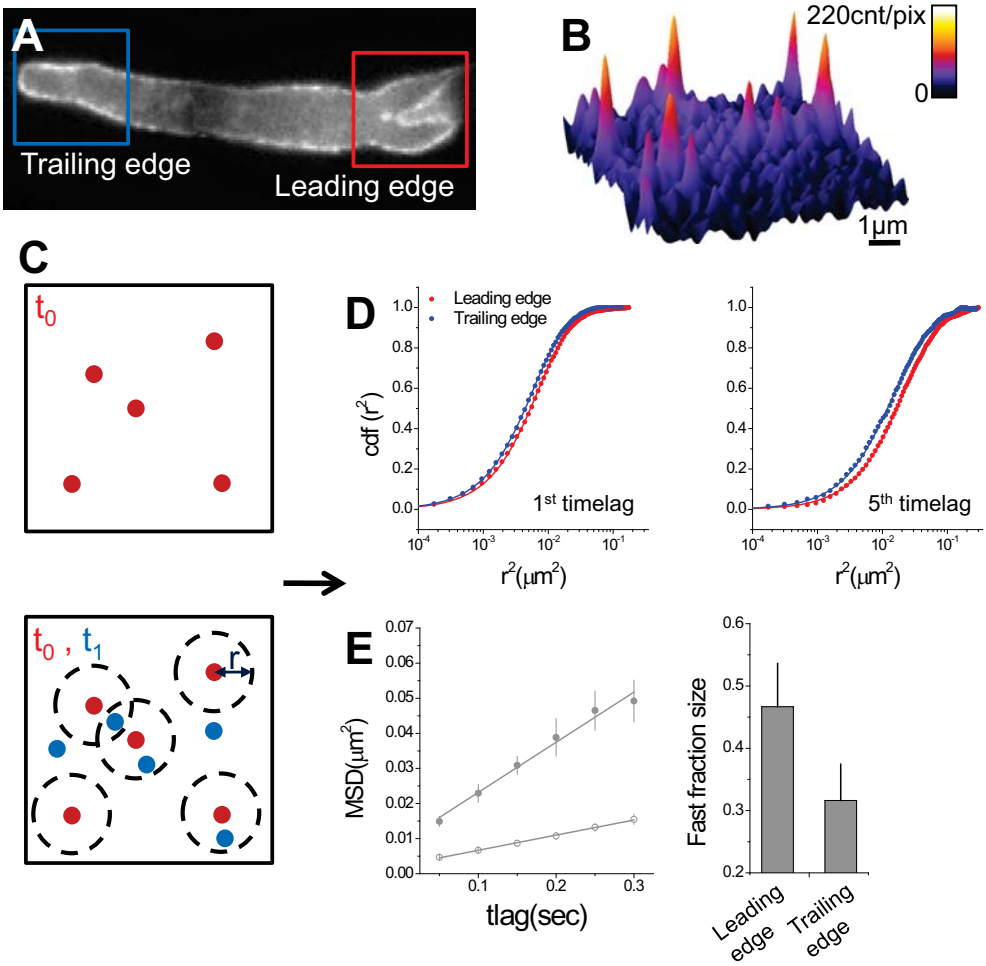
A
Trailing edge
Leading edge
B
220cnt/pix
0
1μm
C
t0
t0 , t1
r
D
Leading edge
Trailing edge
cdf (r2)
1st timelag
5th timelag
r2(μm2)
E
MSD(μm2)
tlag(sec)
Fast fraction size
Leading edge
Trailing edge

Figure 3.1: Experimental setup. **(A)** A needle containing 10 μM cAMP is placed at a distance of ∼70 μm from the region in which the measurements are taken creating a gradient estimated at 4nM/μm over the cells. As soon as the needle is placed, the cells start to change their morphologies from amorphous to highly stretched. **(B)** A 514 nm laser is focused on the apical membrane of the leading and trailing edge where we observe individual eYFP tagged molecules with a positional accuracy of around 40 nm, after low pass fast Fourier transform filtering. **(C)** The correlation between the images in a stack, typically 500 images / cell with a time lag of 50 ms is calculated using PICS (see section 3.2.7) which yields **(D)** cumulative density plots (cdfs) for each time lag, typically up to 400 ms. Fitting of these plots (eq.2.2) results in two MSDs and a fraction size for each of the fractions which is fitted globally. **(E)** When plotted the slope of the MSD *vs* time lag plots represents the diffusion constant ($D = \frac{4t_{lag}}{MSD}$). By assuming the diffusion to be the same between two datasets, the fraction size, α (eq.3.1), becomes the sole parameter that measures the difference between them.

3.3 Results

3.3.1 In naïve wt cells cAR1 moves slowly and exists in two distinct states

Naïve Ax2 (wt) *Dictyostelium discoideum* cells after having been starved for 6 hr. and challenged by cAMP pulsing were very amorphous in shape and spread out readily on the coverglass. Pseudpods seemed to be generated at random as the cells probed their environment (fig.3.2A). Cells initially moved at random.

The mobility of cAR1-eYFP in these cells was investigated on long timescales (up to 400 ms) to get an idea of cAR1 mobility and possible membrane structures or domains that could influence diffusivity. This data will serve as a control for the data presented in what follows. The mean square displacements for given time lags between 50 and 400 ms were determined by PICS that yielded the distribution of square displacements (fig.3.1D). Fitting of those distributions to a diffusion model (eq.3.1) confirmed the existence of two distinct, slow and fast, cAR1 fractions as has been reported earlier [17]. Taking into account the difference in positional accuracy, the mean squared displacements (MSDs) for a timelag of 50 ms MSD_1 = 0.017 $\pm$ 0.002 μm^2 and MSD_2 = 0.005 $\pm$ 0.004μm^2 matched the values reported by de Keijzer and others for a time lag of 44 ms [17]. The linear relation between both MSDs and timelag (fig.3.2B) showed that cAR1 mobility was random, and was characterized by the diffusion constants D_1 = 0.015 $\pm$ 0.002 $\mu m^2/s$ (α = 0.45 $\pm$ 0.06) and D_2 = 0.007 $\pm$ 0.001 $\mu m^2/s$ (1-α = 0.55 $\pm$ 0.06), respectively. The diffusion constant of the fast fraction, D_1, reported here differs significantly from the earlier estimate [17] as obtained from one MSD value at 44 ms only. The latter overestimation was due to the underestimation of the effect of a wide distribution in the positional accuracies by which individual molecules were detected (see also section 3.2.7 and the Appendix). The diffusion constants we found by the more elaborate study here are in line with typical values found for GPCRs [90, 2] in cell membranes. It should be noted that the diffusion of the fast fraction (D=0.015 $\pm$ 0.002 $\mu m^2/s$) closely resembles that of the slow fraction of the G protein heterotrimer (chapter 2). Hence, we suggest that the fast fraction reflects receptors that are pre-coupled to their respective G protein.

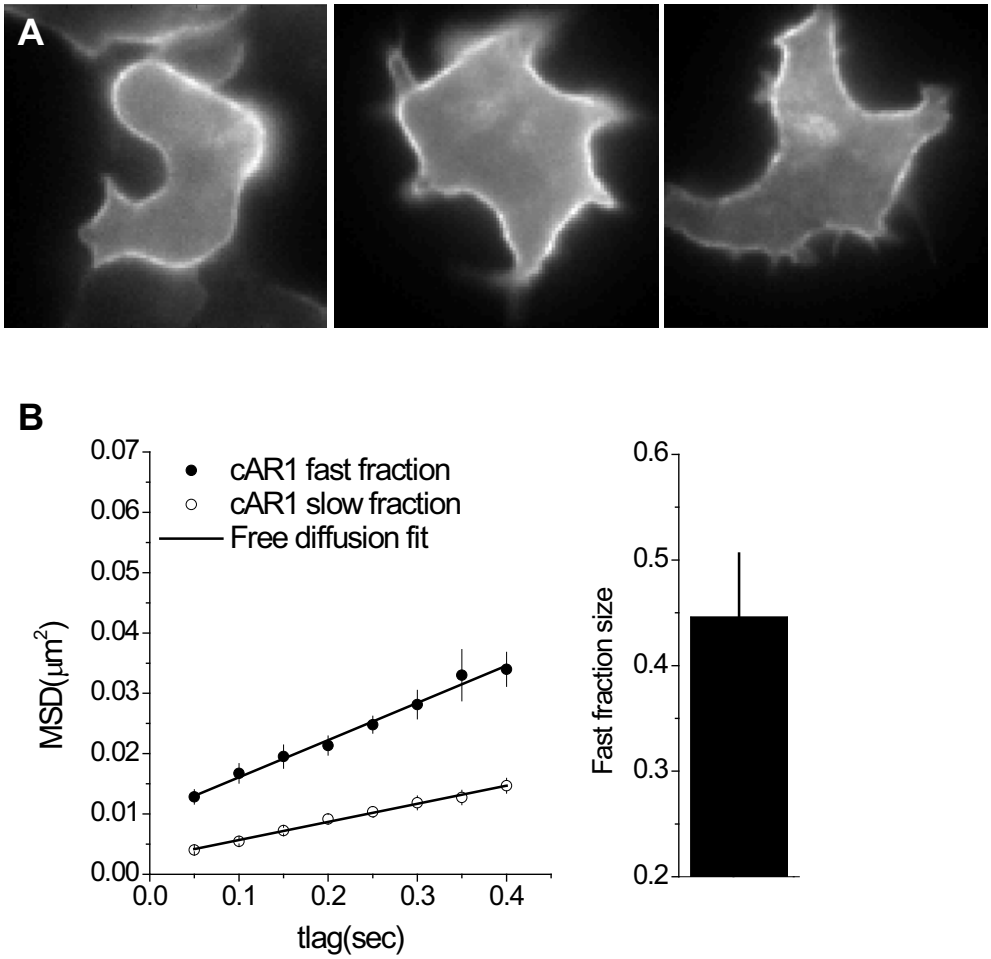

Figure 3.2: Diffusion of cAR1 in naïve wt cells. **(A)** After settling on the coverglass, cells flatten out and extend pseudopods as if exploring their surroundings. **(B)** cAR1 exists in two states with one diffusion constant ∼twofold higher compared to the slower one. The offset difference is explained by a wide distribution of the positional accuracy with which individual molecules are located.

3.3.2 The mobility of cAR1 is polarized and increased in chemotaxing cells

We have previously shown that the mobility of cAR1, as characterized by the MSD after a time lag of 44 ms, was polarized [17]. 23% more fast moving receptors were found at the leading edge of cells as compared to the posterior when cells underwent chemotaxis. In the current paper we set out to characterize the diffusion of cAR1 on longer timescales from 50 up to 400 ms. In this way we intended to retrieve additional details on receptor mobility that in turn is taken as indicator for the local structure of the plasma membrane and its potential restructuring following gradient detection.

Upon application of the cAMP gradient the cells attain a highly stretched morphology (fig.3.3A). We measured > 200 cells and constructed the anterior and posterior cdfs for 6 timelags between 50 and 300 ms. Clearly, the receptor mobility at the anterior was increased with respect to that at the posterior (fig.3.7). Furthermore, we confirmed that the two-fraction model was sufficient to interpret the data. We assumed that the mobility per fraction was identical at the anterior as compared to the posterior. The latter assumption was confirmed by independent fit of the anterior/posterior displacement data that yielded equivalent diffusion constants for both fractions (data not shown). The final result of this advanced analysis confirmed our previous results [17]: cAR1 mobility was higher at the anterior as compared to the posterior. We interpret this higher mobility as an increase in fast fraction size (α in eq.3.1). In this two-fraction interpretation the fast fraction was α = 0.47 $\pm$ 0.05 at the anterior as compared to α = 0.32 $\pm$ 0.05 at the posterior, hence higher by a factor of $\sim$1.5. As compared to naïve cells the diffusion constants of both fractions were also increased twofold to D_1= 0.036 $\pm$ 0.005 $\mu m^2/s$, and D_2= 0.011 $\pm$ 0.001 $\mu m^2/s$, respectively. In comparison to studies on the G proteins (chapter 2), receptor diffusion did not show confinement, at least up to a length scale of 0.05 μm^2, not even upon activation (data not show). That finding might not be surprising given our earlier finding that confinement in G protein mobility was observed at a length scale of 0.6 μm^2.

Cell movements did not influence the values we report here. A cell crawls at a speed of v $\sim$5 µm/min equivalent to $\sim$4 nm/50 ms, which is significantly lower than positional accuracy at which we detected individual molecules. Clearly, at much

longer timelags ($t_{lag} > \frac{4D}{v^2}$ = 23 sec) the linear displacement of the cell would be comparable to that of the molecules (the MSD quadratically increases with time for linear movement). Such timescales were outside of our experimental reach. In addition, the squared displacements parallel to the direction of cell motility was identical to that in the perpendicular direction (data not shown) yet another strong indicator for random cAR1 movement.

3.3.3 cAR1 mobility is not influenced by Gα2 or G$\beta\gamma$ binding

When comparing the mobility of cAR1 between front and back of wt cells performing chemotaxis, the anterior mobile fraction was increased by 15% (fig.3.3, gray bars). In our previous paper we suggested that this anterior cAR1 mobility shift was directly related to Gα2 uncoupling following receptor stimulation. We further suggested that Gα2 by itself was bound to some (potentially) cytoskeleton, structure in order to explain the difference in anterior/posterior mobility [17]. In a follow-up study we characterized the molecular movement of both the Gα2 and the G$\beta\gamma$ subunits of the G protein heterotrimer by which we were able to confirm the coupling of Gα2 to cAR1. It should be noted however that the majority of the G protein heterotrimers ($\sim$70%) was with high certainty uncoupled from cAR1 (chapter 2).

Upon establishment of the full MSD *vs* time curve of cAR1 in the $g\alpha2^-$ cell line, we found no statistically relevant difference (fig.3.4A) in comparison to wt cells. Within experimental uncertainty the diffusion constants were identical for both cell types (fig.3.4A; D_1 = 0.019 $\pm$ 0.003 µm^2/s, D_2 = 0.007 $\pm$ 0.001 µm^2/s). The same holds true for cAR1 mobility in $g\beta^-$ cells (fig.3.4C; D_1 = 0.014 $\pm$ 0.003 µm^2/s, D_2 =0.007 $\pm$ 0.001 µm^2/s, α = 0.39 $\pm$ 0.05). Both findings were in contrast to what we predicted from our earlier studies [17]. Our new, more detailed study shows that the diffusion of cAR1 in $g\alpha2^-$ cells deviates only slightly from that in wt cells, but it does not resemble the diffusion in the leading edge of chemotaxing cells. The loss of polarized cAR1 mobility in $g\alpha2^-$ cells, as reported earlier at the 44 ms timescale [17] however was clearly confirmed here on timescales up to 300 ms. The anterior/posterior mobility difference as seen in the squared displacement distribution in wt cells (fig.3.7) was lost in $g\alpha2^-$ (fig.3.8). A detailed analysis of the mobility showed that the mobile fraction difference for the anterior/posterior cAR1 mobility

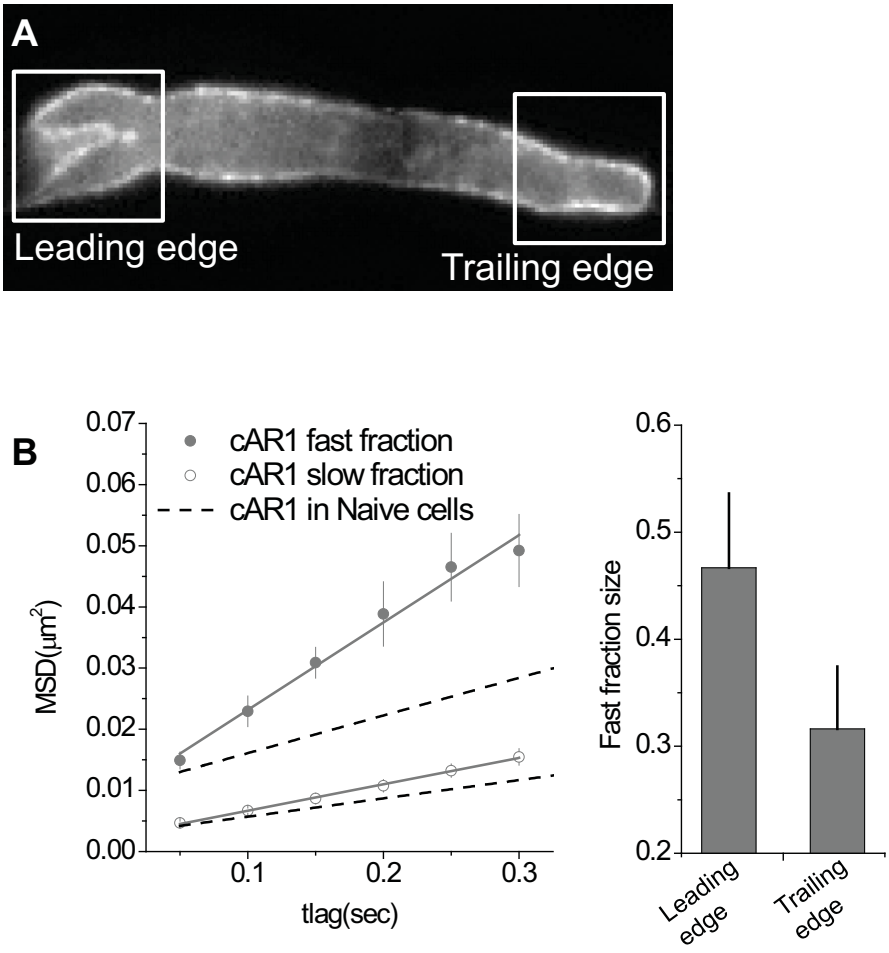

Figure 3.3: Diffusion of cAR1 is polarized and increased in chemotaxing cells. (A) In a gradient, cells attain a highly polarized morphology with a clearly distinguishable leading and trailing edge. **(B)** We fitted the data using a model which assumed the diffusion of both cAR1 fractions to be the same for the leading and trailing edge of a cell (gray dots) and left the fast fraction size (α in eq.3.1, see section 3.2) as the only free parameter which defines the front back difference (gray bars). The overall mobility of cAR1 is significantly higher when compared to the mobility in naïve wt cells (black dashed line). The mobility is higher at the leading edge.

was reduced to 7% (α = 0.36 $\pm$ 0.04 *vs* 0.29 $\pm$ 0.04) as compared to $\Delta\alpha$ = 0.15 (15%) in wt cells (fig.3.4B, compare blue and grey bars; fig.3.8). Interestingly, also the increase in diffusion constants found for wt cells placed into a gradient disappeared for cAR1 in $g\alpha2^-$ cells. The diffusion constants found for $g\alpha2^-$ cells in a gradient were indistinguishable to those found in naïve cells (fig.3.4B); D_1 = 0.016 $\pm$ 0.002 $\mu m^2/s$, D_2 = 0.006 $\pm$ 0.001 $\mu m^2/s$). Together those findings suggest that cytoskeleton rearrangements, which are at the base of the change in cAR1 mobility in polarized wt cells, were impaired in the Gα2 knockout.

3.3.4 Polarized cAR1 mobility is F-actin independent

We investigated whether cAR1 mobility and the mobility shift observed in a gradient was the result of F-actin cytoskeleton rearrangements. Using 0.5 µM lat A F-actin polymerization was inhibited. Wt cells incubated for 10 min with 0.5 µM lat A changed their morphology from amorphous to nearly circular (fig.3.5A). The cells were still able to move albeit at a greatly reduced speed and by extending very small and few pseudopods. It might be interesting to note that at the bottom membrane intact cytoskeleton structures were still present (fig.3.5B). That latter observation further ensured us to pursue experiments on the apical membrane of the cell, as compared to experiments performed by many other groups that only address the basal membrane by total-internal reflection microscopy.

After lat A treatment, the diffusion constants of both cAR1 fractions increased twofold to D_1= 0.028 $\pm$ 0.006 $\mu m^2/s$ and D_2= 0.015 $\pm$ 0.002 $\mu m^2/s$ (fig.3.5C, green dots), when compared to naïve wt cells, whereas the mobile fraction slightly decreased to α = 0.38 $\pm$ 0.05 (fig.3.5C, green bar). Both findings were nearly identical to values obtained for wt cells in a cAMP gradient (fig.3.5C, gray dashed line). These results indicate that indeed cAR1 mobility is modulated by F-actin interactions.

To see if absence of the F-actin polymerization also abolished the polarity of cAR1 mobility in a gradient, we applied a cAMP gradient to lat A treated cells. In the gradient cells were not able to take on the elongated shape but were morphologically indistinguishable from lat A treated cells without the challenge (fig.3.5A). The mobility shift that was observed in untreated cells prevailed. We found a difference in fast fraction size in lat A treated cells of 14$\pm$7% between anterior (43 $\pm$ 6%) and

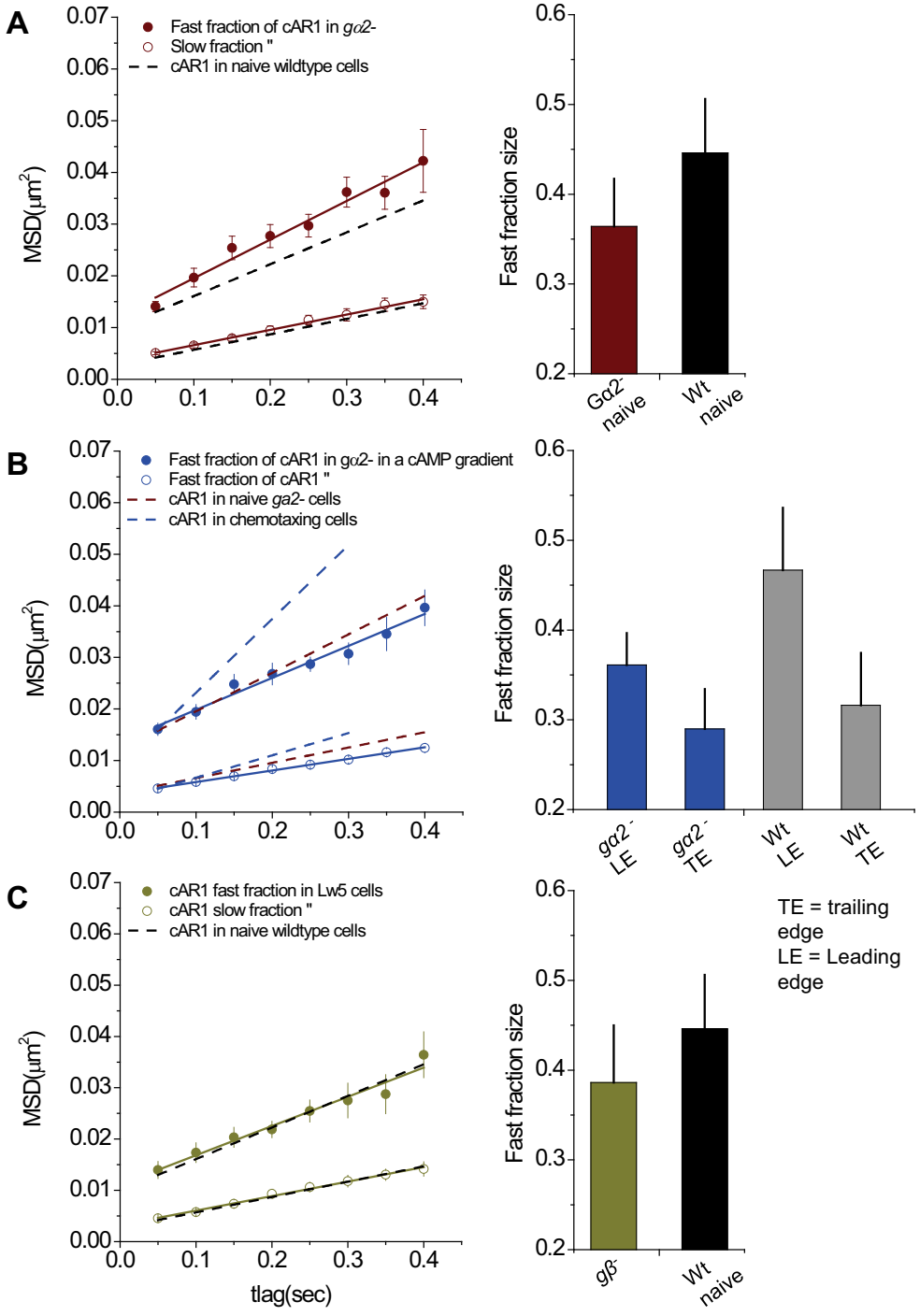
A
Fast fraction of cAR1 in gα2-
Slow fraction "
cAR1 in naive wildtype cells
MSD(μm²)
Fast fraction size
Gα2- naive
Wt naive
B
Fast fraction of cAR1 in gα2- in a cAMP gradient
Fast fraction of cAR1 "
cAR1 in naive ga2- cells
cAR1 in chemotaxing cells
MSD(μm²)
Fast fraction size
gα2- LE
gα2- TE
Wt LE
Wt TE
C
cAR1 fast fraction in Lw5 cells
cAR1 slow fraction "
cAR1 in naive wildtype cells
MSD(μm²)
tlag(sec)
Fast fraction size
gβ-
Wt naive
TE = trailing edge
LE = Leading edge

Figure 3.4: The G-protein does not affect cAR1 mobility but is needed for the mobility increase during chemotaxis. Comparison of the mobility of cAR1 in wt (black dashed line, black bar) with the mobility in the absence of Gα2 (wine dots, wine bar) does not reveal any difference. **(B)** When the $g\alpha 2^-$ cells are placed in gradient, cAR1 does not increase its mobility (blue dots) compared to wt cells in a gradient (black dashed line) but remains the same as in naïve $g\alpha 2^-$ cells (wine dashed line), the fraction size difference between front/back decreases to $\sim 8\%$ **(C)** knocking out Gβ also has no effect on the movement of cAR1 (yellow dots, yellow bar) when compared to its movement in wt cells (black dashed line, black bar).

posterior (29 $\pm$ 8%) (fig.3.5D, compare red bars, fig.3.9). Likewise the diffusion constants increased to D_1 = 0.058 $\pm$ 0.012 $\mu m^2/s$ and D_2 = 0.013 $\pm$ 0.001 $\mu m^2/s$.

Hence, the increase in mobility that was found in untreated wt cells on stimulation in a cAMP gradient (fig.3.3) was governed by actin-related cell-cortex components that presumably hinder free cAR1 movement in the cell membrane however; F-actin appears not to be the only cortex/membrane component to attenuate cAR1 mobility. As expected, treatment of $g\alpha 2^-$ cells with lat A gives an identical result as in wt cells indicating that an intact G protein is important for cortex remodeling, required for chemotaxis, but not for basic cortex functioning, as suggested before [80].

3.4 Discussion

As reported earlier [17], in naïve *D. discoideum* cells two fractions of the cAMP receptor cAR1 can be distinguished that differ in their mobility characterized by the diffusion constants of D_1 = 0.015 $\pm$ 0.002 $\mu m^2/s$ for the fast, and D_2 = 0.007 $\pm$ 0.001 $\mu m^2/s$ for the slow fraction, respectively. Those values are in line with previously reported diffusion constants for cAR1 [90], and more generally on G protein coupled receptors [2].

When naïve wt cells were subjected to a cAMP gradient they attained a polarized morphology, and the overall mobility of cAR1 increases about twofold with a clear polarized increase when leading and trailing edge were compared. Our data showed that the mobility of cAR1 and its polarized nature is largely controlled by the cytoskeleton, specifically by F-actin but most likely also other membrane components. The mobility of cAR1 appeared to be a measure for the strength of the underlying cortex-membrane interactions. These interactions were weaker at the anterior of cells crawling in a cAMP gradient than at the posterior which is reflected by the higher cAR1 mobility at the leading edge. It has been reported earlier that the cell cortex is heavily remodeled during chemotaxis [33], and that interactions between GPCRs and F-actin play a role in signaling [86, 2]. Actin cortex - membrane interactions were found to be largely polarized in chemotaxing *D. discoideum* cells [64, 17] and evidence for direct binding of a cAMP receptor to F-actin in *D. discoideum* has been reported [31].

To test whether F-actin was influencing the mobility of cAR1 we incubated the naïve cells with lat A. Indeed, after this treatment the mobility of both receptor fractions increased twofold, reminiscent of the mobility increase in chemotaxing cells. Hence, the modulation of cAR1 mobility was clearly F-actin dependent and must rely on some direct or indirect receptor-actin interaction. The exact nature of the interaction remains elusive though. Several scenarios can be thought of that explain our data. First, fast, transient binding of cAR1 either directly or indirectly to F-actin bundles that line the membrane may explain the relatively low mobility in naïve cells. If these interactions proceed at much faster timescales than the time lag in our measurements (50 ms) the binding/unbinding kinetics will be observed as slower diffusion. Second, cAR1 might be confined to very small F-actin related domains also called corrals [56] (visualized by Morone and others [66]). Hence, the actual diffusion we observed was rather the macroscopic diffusion of cAR1, a result of the fast microscopic diffusion within small corals and a given probability of hopping from coral to coral. If the corals are small and the microscopic diffusion fast, such corals cannot be resolved by our slow (50 ms) technique [98]. Actually, we found evidence of corrals in the diffusion of the G protein subunits (chapter 2) however the average size was $\sim$600 nm, too large to hinder the diffusion of cAR1 in a way that we could observe. A third explanation could be that one fraction of cAR1 was directly bound to F-actin and its movement was thereby determined by the movement of F-actin fibers. This latter possibility appears unlikely as we have shown that the Gβ subunit of the G protein immobilizes completely via F-actin and as such was characterized by a diffusion constant of < 0.002 $\mu m^2/s$, 3 times slower than that of the slow fraction of cAR1.

From these results however, a paradox arises. Although F-actin decreased the mobility of cAR1, we measured a mobility increase in the F-actin rich leading edge of chemotaxing cells. One would expect the mobility to decrease in the presence of high F-actin abundance. This apparent paradox may be explained by differential F-actin membrane interactions though. The fact that F-actin accumulates at the leading edge does not imply that it lines the membrane or that it interacts with membrane molecules. In fact, Merkel and others showed that there is a significant weakening of the cortex-membrane interactions at the anterior during chemotaxis. It was reported that in a *talin* knock-out cell line the posterior of the cell shows the same low level

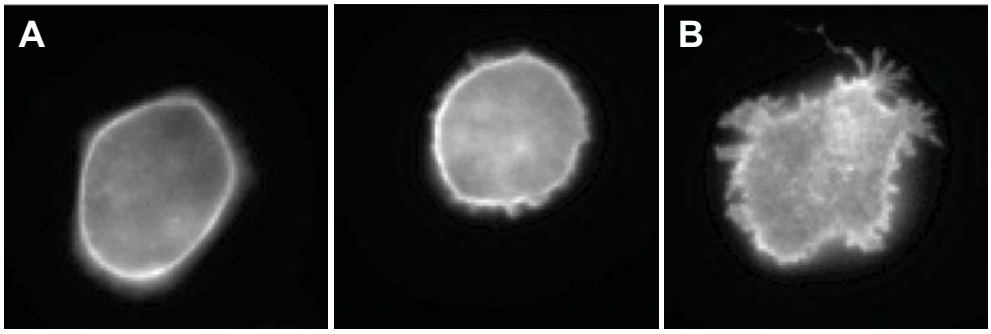
A
B

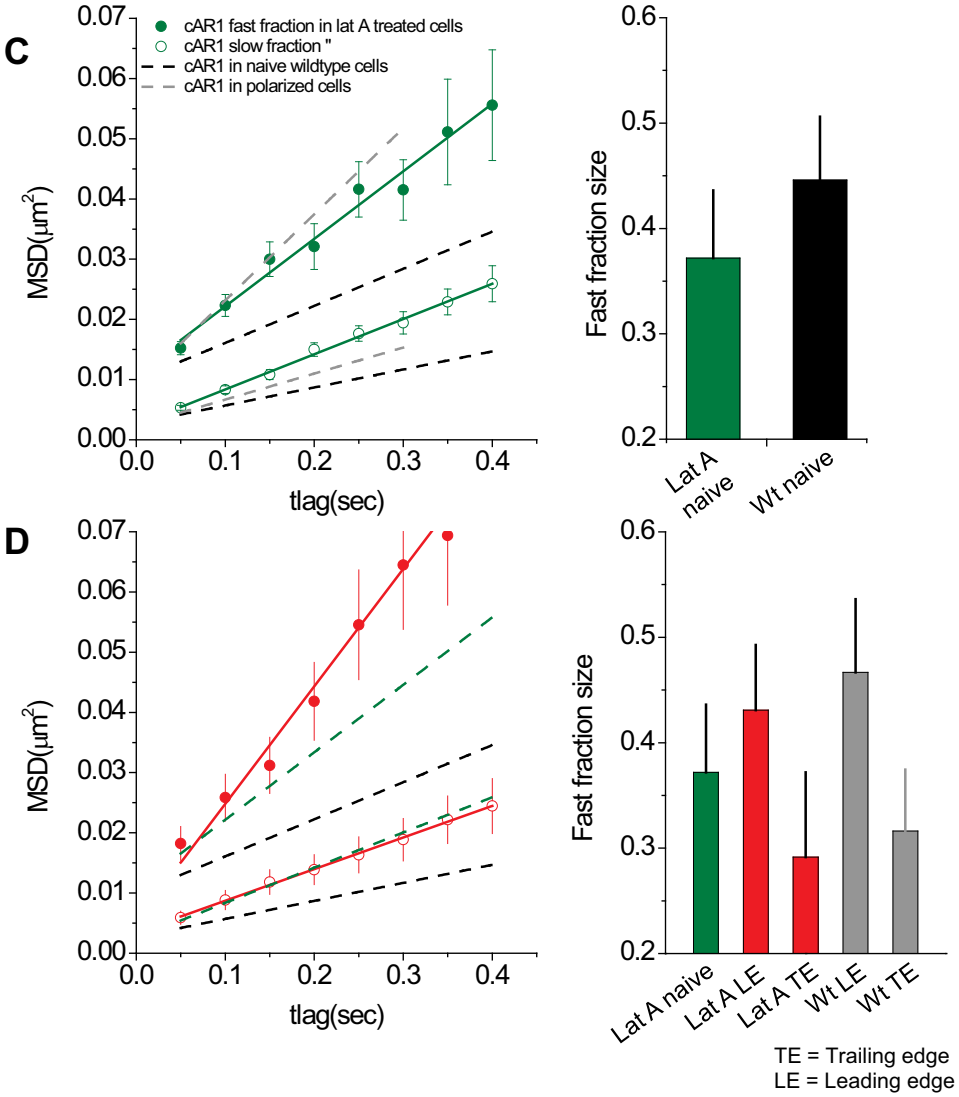
C
cAR1 fast fraction in lat A treated cells
cAR1 slow fraction "
cAR1 in naive wildtype cells
cAR1 in polarized cells
MSD(μm²)
tlag(sec)
Fast fraction size
Lat A naive
Wt naive
D
MSD(μm²)
tlag(sec)
Fast fraction size
Lat A naive
Lat A LE
Lat A TE
Wt LE
Wt TE
TE = Trailing edge
LE = Leading edge

Figure 3.5: Inhibition of F-actin polymerization leads to higher cAR1 mobility but not the loss of polarized mobility. **(A)** Lat A treated cells lose their amorphous shapes and become nearly round, **(B)** at the bottom membrane however, intact cytoskeleton structures can still be observed. **(C)** Naïve lat A treated wt cells show a higher cAR1 mobility for both fractions (green dots) then naïve cells with an intact cytoskeleton (black dashed line). **(D)** When placing lat A treated cells in a cAMP gradient the overall mobility goes up (red dots) with respect to naïve lat A treated cells (green dashed line). Assuming diffusion between leading edge and trailing edge to be equal, the mobility polarization (red bars) is of the same magnitude as that found in untreated cells in a gradient (black bars), the fast fraction size of naïve lat A treated cell is plotted for comparison (green bar).

of actin-membrane coupling as the anterior [64]. The tighter interaction between the cytoskeleton and the membrane at the posterior probably has a function in myosin mediated trailing edge-retraction [64]. The attenuation of the membrane-cortex interaction at the leading edge may thereby facilitate the production of blebs, a mechanism for amoeboids to obtain high crawling speeds [101]. In addition two types of F-actin have been observed at the leading edge of lung epithelial cells and kidney epithelial cells [73]. Likely, both types are abundant in chemotaxing *Dictyostelium* cells. The actin that is responsible for the protrusion of the membrane and is more abundant at the anterior does not lead to tight actin-membrane interactions, whereas the actin that is responsible for the structure of the membrane cortex is weakened there. In light of these results we can understand how the mobility of cAR1 can be polarized; due to the differential cortex-membrane interactions and the decoupling of the cytoskeleton from the membrane specifically at the leading edge. Such interpretation is further supported by our surprising finding that polarized cAR1 mobility was also found in F-actin-depleted cells. Probably the cortex filaments other than F-actin also influence cAR1 mobility. It was shown that removing F-actin (treatment with 7.5 µM latrunculin B) still leaves cells with an actively regulated cortex [33].

We further found that the polarization in cAR1 mobility was Gα2 dependent, as the anterior/posterior mobility shift disappeared in $g\alpha 2^-$ cells. Moreover, the overall mobility of cAR1 did not increase upon gradient application. Both results indicate that the restructuring of the cytoskeleton required for chemotaxis does not take place in this knockout, not surprising since chemotactic signaling is abolished. An intact G protein does not seem to be a prerequisite for the formation of pseudopods and random cell movement. For polarization and directional movement though, a fully functional G protein is required [99, 80]. The fact that cAR1 mobility in lat A treated $g\alpha 2^2$ cells reflects lat A treated wt cells supports that indeed, these cells seem to have normal basal cortex functionality (data not shown).

In conclusion we have shown that cortical F-actin restricts cAR1 movement but it is probably not the only cortex component responsible. Naïve wt as well as $g\alpha 2^-$ cells exhibit a relatively tight membrane - cortex interaction resulting in low cAR1 mobility. We have shown before (chapter 2) that in naïve cells a large portion of the receptors ($\sim$45%) were coupled to their heterotrimeric G protein (fig.3.6A). When

the cells polarize and form a leading edge, a tight cortex-membrane interaction at the anterior would be counter-productive, first because the cortex itself is a major substrate for force generation, and second a less tight membrane - cortex interaction facilitates blebbing mediated motility [101, 58]. It is known that the cortex is weakened at the anterior [64] and that a direct link between cAR1 and cortex components is likely [31]. On the other hand, cortex - membrane connections should be favored at the posterior to allow for myosin II mediated contraction of the uropod [89]. We propose a model in which the mobility of the receptor is governed by F-actin interactions (fig.3.6A). In chemotaxing cells cAR1 mobility is polarized due to the polarized configuration of the cortical F-actin cytoskeleton that interacts with the membrane (fig.3.6B). The anterior and the lateral sides of the cell are lined with an F-actin cortex. This cortex is broken down specifically at the leading edge to facilitate bleb formation and F-actin force generation.

We characterized the molecular motion of cAR1 and showed that this motion is a direct reflection of the underlying cortex - membrane structure. Potentially regulation of the F-actin cytoskeleton goes two ways. Initially the actin polymerization is stimulated by the receptor - G protein system and subsequently F-actin regulates the mobility of both molecules which facilitates their localization and could increase their local concentration. This might help cells to define their direction with respect to an external chemical gradient.

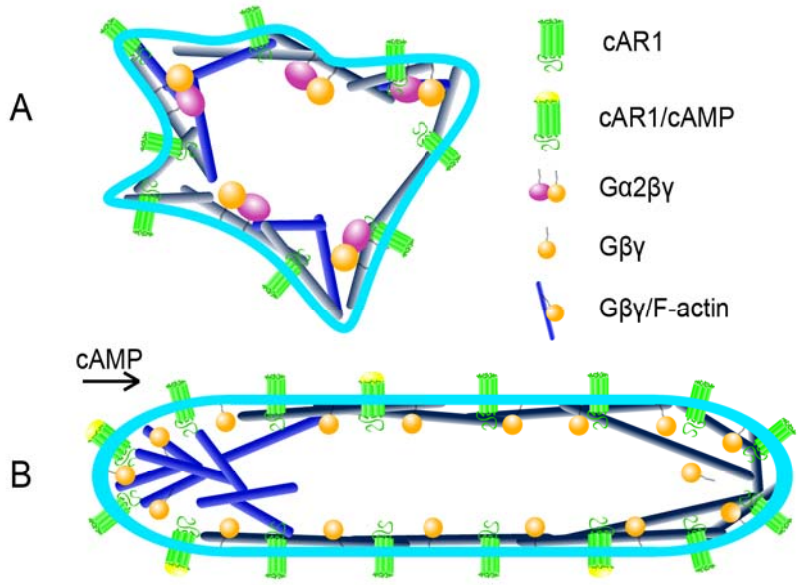

Figure 3.6: A model explaining the results. **(A)** Naïve cells are amorphous; they move randomly and have tight cytoskeleton - membrane interactions. Pseudopods are extended at random but don't persist for very long, as if the cells probe the environment. The cAR1 molecules are restricted in their diffusion by the membrane cytoskeleton. A minority (∼30%) of the membrane associated G protein $\alpha 2$ and $\beta\gamma$ subunits appear to move together with a portion of the cAR1 molecules. **(B)** Upon application of a cAMP gradient, the cells polarize and attain highly elongated shapes. The increase of the overall mobility is explained by F-actin cortex rearrangements which take place in chemotaxing cells. The polarized mobility is explained by the polarized configuration of the cortex. At the leading edge the cortex is broken down or restructured, possibly mediated by talin [64]. This allows for the formation of blebs driven by hydrostatic forces and facilitates growth of the F-actin cytoskeleton [101, 58]. At the leading edge a tight cortex - membrane interaction would obstruct movement whereas at the trailing edge these interactions are needed for the retraction of the uropod. $G\beta\gamma$ as well as $G\alpha 2$ knock out cells remain as in **(A)** upon exposure to a stable cAMP gradient.

Supplemental information

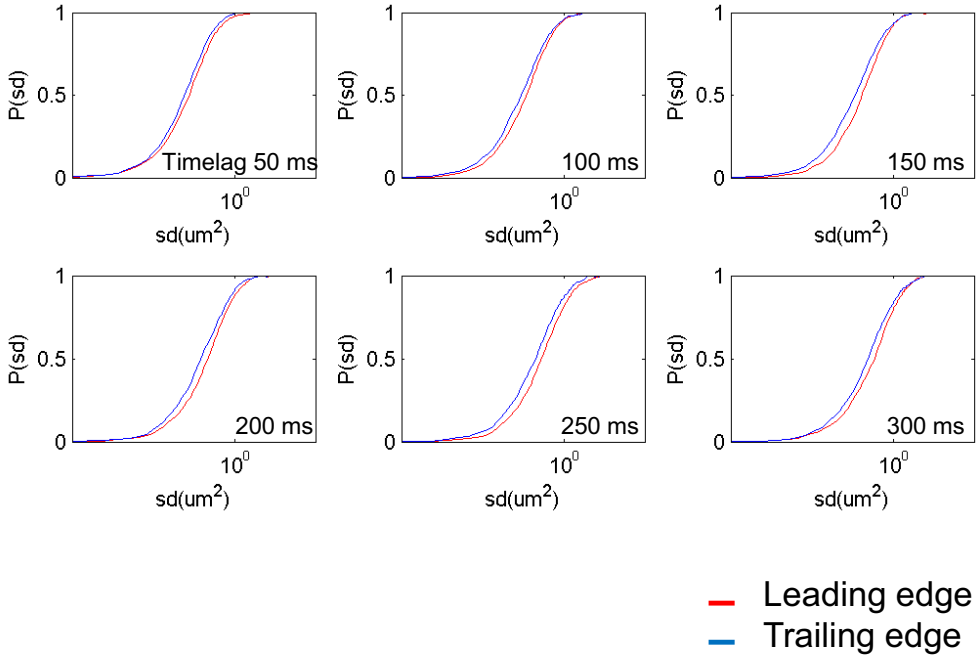

Figure 3.7: Mobility polarization without applying a model. The raw P(sd) plots (cdfs) clearly show the mobility polarization between the anterior and posterior of wt cells in a cAMP gradient. These cdfs are interpreted as showing the same two diffusion constants but differ in their fraction size distribution by fitting with the biexponential function as described in section 3.2.

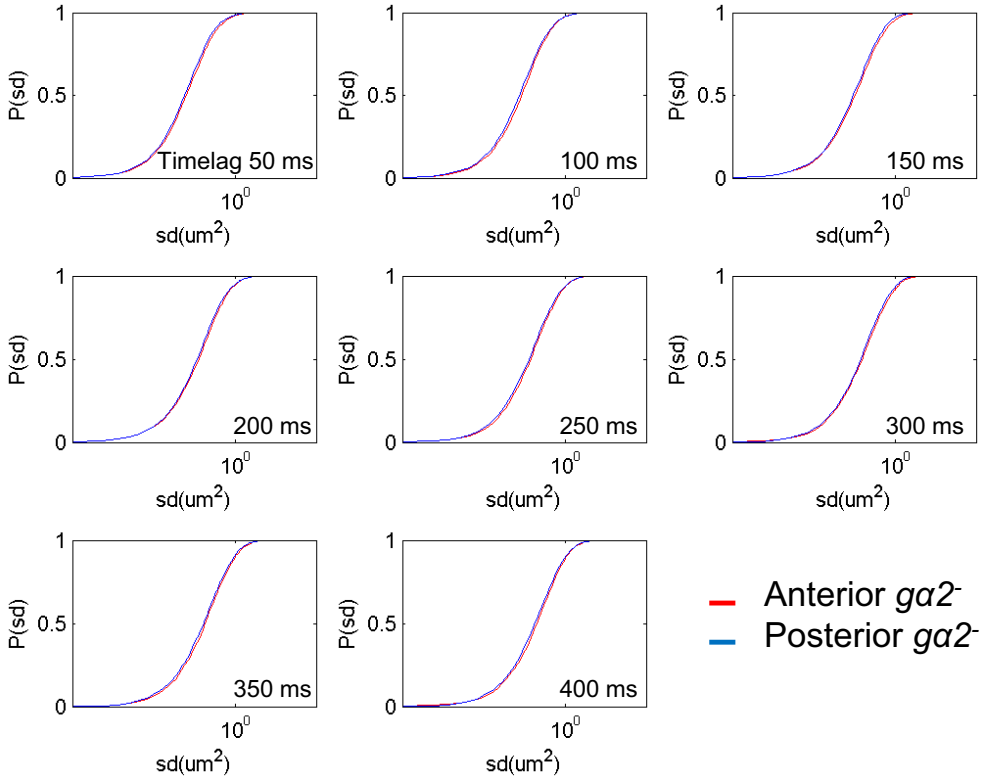

Figure 3.8: Gα2 knockout cells lose polarized cAR1 mobility. The cAR1 mobility difference between the part of the $g\alpha 2^{-}$ cells closest to and that furthest away from the needle is negligable.

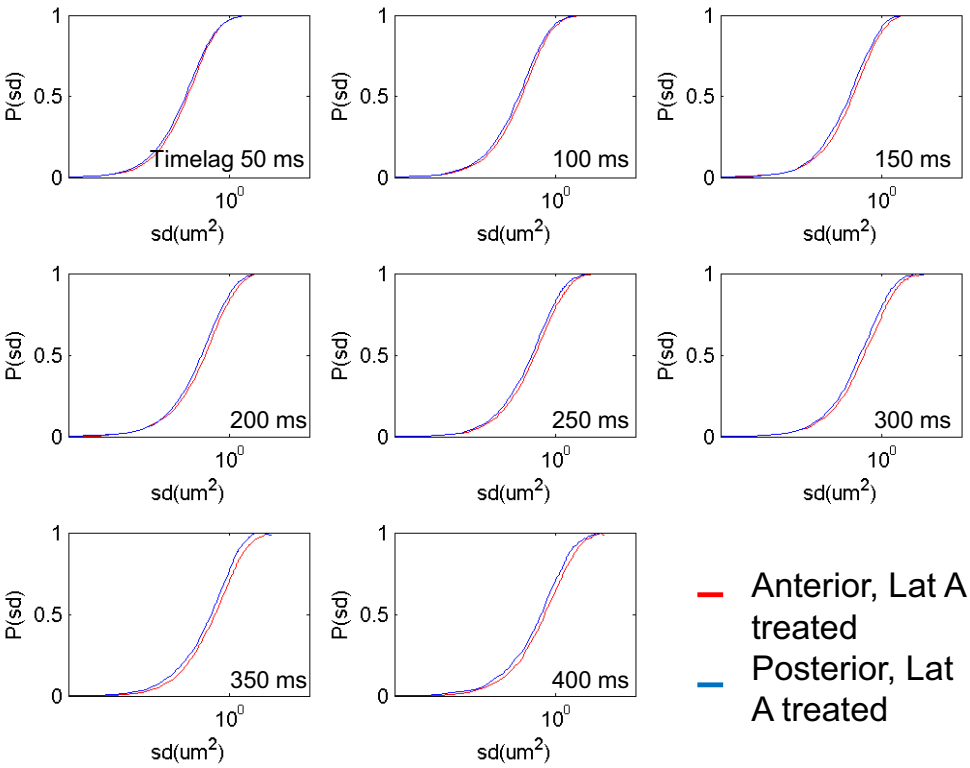

Figure 3.9: Mobility is still polarized after lat A treatment. Despite inhibition of actin polymerization using lat A, a significant mobility shift is still observed between the anterior and posterior of the cells.

Appendix

The distribution of squared displacements, sd, characterized by a mean squared displacement, MSD, and positional accuracy, σ, assuming a random walk in two dimensions is given by [82, 10]:

$$p(sd) = \frac{1}{\sqrt{\pi(MSD + 4\sigma^2)}} \frac{1}{\sqrt{sd}} \exp\left(- \frac{sd^2}{MSD + 4\sigma^2} \right) \tag{3.3}$$

Integration of equation 3.3 from the origin to r^2 leads to the expression of the cumulative distribution function $cdf(r^2)$ found in equation 2.1. In the derivation of eqations 3.1, 3.2& 3.3 it was assumed that the accuracy by which the position of the molecules, σ is determined in each dimension is a constant. However, given that σ scales with the signal-to-noise ratio ($\sigma = \frac{\lambda}{2\sqrt{SNR}}$, λ wavelength of light), and since every observation of an individual molecule is achieved at different signal-to-noise ratio, a distribution in σ must be taken into account. The experimental data show that the distribution in σ is sufficiently represented by a Gaussian of mean σ_0 = 40 nm and width δ_σ = 20 nm (fig.3.10A):

$$p(\sigma) = \frac{1}{\sqrt{2\pi}\delta_\sigma} \exp\left(- \frac{(\sigma - \sigma_0)^2}{2\delta_\sigma^2} \right) \tag{3.4}$$

Hence for a proper treatment of the problem the distribution in positional accuracy must be taken into account as a convolution of equation 3.3 and 3.4. For the cumulative distribution function convolution results in:

$$cdf(r^2) = \frac{1}{\sqrt{2\pi}\delta_\sigma} \int_0^\infty d\sigma \exp\left(- \frac{(\sigma - \sigma_0)^2}{2\delta_\sigma^2} \right) \left(1 - \exp\left(- \frac{r^2}{MSD + 4\sigma^2} \right) \right) \tag{3.5}$$

Equation 3.5 approaches for a narrow distribution in positional accuracy ($\delta_\sigma \ll \sigma$) or for large MSDs (MSD $\gg 4\sigma^2$), $cdf(r^2) = 1 - \exp\frac{-r^2}{MSD+4\sigma^2}$, the solution found in equation 2.1. In both cases the positional offset is given by $s_0 = 4\sigma_0^2$. In all other cases, as those discussed in the current paper, treatment of the data using equation 3.1 results in values of s_0 that depend on MSD, and hence leads to two different offsets $s_{0,1}$ and $s_{0,2}$ for the two mobile fractions, respectively.

The analysis has been verified by simulation. PICS analysis has been performed on simulated data of single-molecule diffusion assuming a fast and a slow fraction and in which the width in positional accuracy, σ_σ, was varied. The results are summarized in figure 3.10B. The dependence of s_0 on δ_σ is clearly revealed.

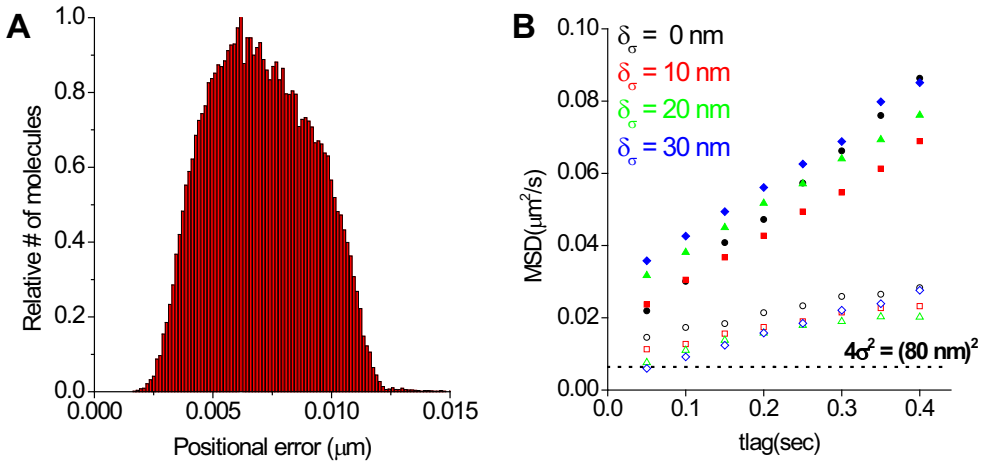

Figure 3.10: The distribution of positional accuracies leads to an offset difference in the two diffusing fractions .